

Modeling of spaced-receiver scintillation measurements

A. W. Wernik,<sup>1</sup> C. H. Liu, and K. C. Yeh

University of Illinois at Urbana-Champaign

(Received March 1, 1983; accepted May 20, 1983.)

Spaced-receiver scintillation measurements are modeled applying scintillation theory together with model spectral representations of nonfrozen turbulent media. The effects of velocity distribution of scatterers, diffusion of irregularities and velocity gradient across the scattering layer on parameters derived from spaced-receiver scintillation experiments are studied. Both correlation and dispersion analyses are considered. The results from modeling are compared with observational data from the equatorial region. It will be demonstrated that self-consistent models can be constructed in interpreting the data and information about the drift velocity field in the ionosphere can be obtained from spaced-receiver experiments.

1. INTRODUCTION

The spaced-receiver technique is used extensively to measure the velocity of moving patterns formed on the ground by a radio wave after being scattered by ionospheric irregularities. Most commonly used techniques are the correlation and dispersion analysis of fluctuating signals either reflected from or passing through the irregular ionosphere. There is a large number of papers on the subject including several comprehensive reviews [cf. Briggs, 1968a, b, 1977; Fedor, 1967; Kent and Wright, 1968; Wright and Pitteway, 1978]. The quantities directly available from spaced-received data analysis are the mean drift velocity and its direction, the characteristic random velocity which is a measure of random changes in the pattern, and the spatial scales and orientation of the principal axis of the pattern which can be related to the spatial form and orienta-

tion of the irregularities responsible for the signal fluctuations. Usually the mean drift velocity has been interpreted in terms of the bulk ionization velocities ( $\bar{E} \times \bar{B}$  drift or neutral winds) or in terms of the phase velocities of wave motions, such as gravity waves. Considerably less clear is the meaning of the characteristic random velocity  $V_c$ . It was introduced by Briggs et al. [1950] in a somewhat arbitrary manner without relating it to any specific possible physical mechanisms causing variations of the irregular ionospheric structure, such as fluctuations of the drift velocity, diffusion of irregularities, and the dispersive nature of the motion of the irregularities in the ionosphere. At the same time, it seems apparent that the temporal evolution in the scintillation pattern should reflect important dynamic processes that take place in the turbulent ionosphere and such easily measured parameters as the characteristic random velocity might be useful in studying these processes.

The problem of relating  $V_c$  to its possible causes has been discussed for interplanetary irregularities by Little and Ekers [1971] and Ekers and Little [1971]. Lotova and Chashey [1973, 1976, 1977a, b, 1978, 1981] and Chashey and Shishov [1977]

<sup>1</sup>On leave from Space Research Center.

Copyright 1983 by the American Geophysical Union.

Paper number 3S0861.

0048-6604/83/0910-0861\$08.00

discussed the dispersion analysis applied to interplanetary scintillation. Random motion of scatterers has been incorporated in the numerical simulation of ionospheric drift measurements by Wright and Pitteway [1978]. They have shown that the characteristic random velocity can be identified with the rms value of the scatterers' velocity.

The effect of drift velocity variation along the propagation path has been qualitatively discussed by Briggs and Golley [1968] in reference to the radio star scintillation measurements. They have shown that it may cause a systematic skewness of the cross-correlation function and positive velocity dispersion, i.e., an apparent increase of the drift velocity with frequency.

In the present paper we will use Shkarofsky's [1968] description of the nonfrozen turbulent medium together with the phase screen scintillation theory to model effects of velocity distribution, diffusion, and velocity variations inside the scattering layer on parameters derived from the spaced-receiver scintillation data. Both correlation and dispersion results will be compared with satellite scintillation data taken at Ancon, Peru, near the magnetic equator.

This paper attempts to model quantitatively the spaced-receiver scintillation experiments and to demonstrate that important information about the drift velocity in the ionosphere can be obtained from spaced-receiver scintillation data. In section 2, a brief discussion of the various models of space-time spectra is presented. Correlation analysis based on the models and scintillation theory is derived in section 3. Dispersion analysis using the cross-spectrum is discussed in section 4. In section 5, the modeling results are compared with observational data to demonstrate the self-consistency of the model. Some conclusions are given in section 6.

## 2. STATISTICAL CHARACTERIZATION OF NONFROZEN IRREGULARITIES

In order to model scintillation it is necessary to adequately characterize the irregular medium through which a wave

propagates. Most commonly it is assumed that the electron density fluctuation  $\Delta N(\mathbf{r})$  is a random function of position, sufficiently described by its first two moments: mean and autocorrelation. If all irregularities move with a constant velocity and do not vary with time (so called "frozen-in" assumption or Taylor hypothesis), spatial and temporal characteristics of the medium are related by a simple translation of the motion [cf. Tatarski, 1971; Rino and Livingston, 1982; Yeh and Liu, 1982]. In reality, however, the electron density fluctuations vary also in time and the frozen-in assumption may not be valid. Several processes might be responsible for the violation of the frozen-in assumption, such as (1) regular, temporal and spatial variations of the drift velocity, (2) dispersive nature of the motion, (3) fluctuations of the drift velocity, and (4) decay of irregularities due to diffusion. The problem is to obtain an adequate representation of these processes, so that they can be easily incorporated into the scintillation theory. A useful representation has been suggested by Shkarofsky [1968]. In his description of the nonfrozen flow of turbulent plasma it is assumed that the outer scale of turbulence, the temporal variations of the generation mechanisms are slow as compared to other mechanisms that can change the space-time structure of the irregularities, such as drift velocity fluctuations or diffusion. With this assumption it is possible to decompose the space-time spectrum of electron density fluctuations  $S_{\Delta N}(\bar{\kappa}, \omega)$  into a spatial part dependent on  $\bar{\kappa}$  only,  $\phi_{\Delta N}(\bar{\kappa})$ , and a part  $\psi(\bar{\kappa}, \omega)$  normalized such that

$$\int_{-\infty}^{\infty} \psi(\bar{\kappa}, \omega) d\omega = 1 \quad (1)$$

Thus

$$S_{\Delta N}(\bar{\kappa}, \omega) = \phi_{\Delta N}(\bar{\kappa}) \cdot \psi(\bar{\kappa}, \omega) \quad (2)$$

$$S_{\Delta N}(\bar{\kappa}, \tau) = \phi_{\Delta N}(\bar{\kappa}) \cdot \psi(\bar{\kappa}, \tau)$$

where  $\phi_{\Delta N}(\bar{\kappa})$  is identified with the usual spatial irregularity spectrum, and  $\psi(\bar{\kappa}, \omega)$  and its temporal Fourier transform  $\psi(\bar{\kappa}, \tau)$  are associated with different decay mech-

anisms. If the flow is strictly frozen with velocity  $\bar{v}_0$  we have

$$\psi(\bar{\kappa}, \omega) = \delta(\omega + \bar{\kappa} \cdot \bar{v}_0) \quad (3)$$

The Fourier transform of  $\psi(\bar{\kappa}, \omega)$  with respect to  $\omega$  gives

$$\psi(\bar{\kappa}, \tau) = e^{-i\bar{\kappa} \cdot \bar{v}_0 \tau} \quad (4)$$

Shkarofsky suggested the following general form of the function  $\psi(\bar{\kappa}, \tau)$ :

$$\psi(\bar{\kappa}, \tau) = e^{-i\bar{\kappa} \cdot \bar{v}_0 \tau - \kappa^2 \Delta^2 / 2} \quad (5)$$

where  $\Delta$  is a function of time and represents the rms displacement of an irregularity in time  $\tau$  due to some decay mechanism. If the decay is caused by drift velocity fluctuations, the so-called "locally frozen" field condition may sometimes apply. Under this condition, the velocity of the individual irregularities can be considered constant over a period short compared with  $L_0/v_0$ , where  $L_0$  is the outer scale of turbulence and  $v_0$  is the mean flow velocity. If these velocity fluctuations are normally distributed with a standard deviation  $\sigma$  of each velocity component, it can be shown that  $\psi(\bar{\kappa}, \tau)$  becomes [Tatarski, 1971]

$$\psi(\bar{\kappa}, \tau) = e^{-i\bar{\kappa} \cdot \bar{v}_0 \tau - \kappa^2 \sigma^2 \tau^2 / 2} \quad (6)$$

Thus, for this case,  $\Delta = \sigma \tau$ .

Equation (6) reduced to the frozen field result (4) if

$$\frac{\sigma^2}{v_0^2} \ll \frac{2}{\kappa^2 v_0} \quad (7)$$

The irregularity size most effective in producing amplitude scintillation is of the order of the Fresnel zone dimension  $\sqrt{\lambda z}$ , where  $\lambda$  is the wavelength and  $z$  is the observer's distance from the irregularity slab. From (7) we see that high-frequency waves are more susceptible to velocity fluctuations than low-frequency waves. Also the high-frequency part of the scintillation spectrum will be more susceptible to nonfrozen flow effects.

Another decay mechanism that might be of importance for ionospheric irregularities

is diffusion leading to temporal variations of the rms electron density fluctuation. For this case, according to Shkarofsky [1968],  $\Delta = \sqrt{2D|\tau|}$  with  $D$  representing the diffusion coefficient. The functions  $\psi(\bar{\kappa}, \tau)$  and  $\psi(\bar{\kappa}, \omega)$  become

$$\psi(\bar{\kappa}, \tau) = e^{-i\bar{\kappa} \cdot \bar{v}_0 \tau - \kappa^2 D |\tau|} \quad (8)$$

$$\psi(\bar{\kappa}, \omega) = \frac{2\kappa^2 D}{(\omega + \bar{\kappa} \cdot \bar{v}_0)^2 + \kappa^4 D^2} \quad (9)$$

The condition for the validity of frozen field can be derived as  $D \ll v_0/\kappa$ , which is independent of time.

So far we have discussed effects of the time decay of turbulence. It turns out that a smooth, regular variation of velocity inside the turbulent layer can also have effects on scintillation. Let us assume that the flow velocity is constant over distances shorter than the outer scale of turbulence  $L_0$ . This means that in a certain region  $G$  with dimensions of the order of  $L_0$ , the field can be considered as frozen and moving with a certain velocity  $\bar{v}_1$ . On passing to another region  $G_2$  at a distance not less than  $L_0$  from  $G_1$ , the field is still frozen and has the same statistics but moves with different velocity  $\bar{v}_2$ . As we mentioned turbulence scintillation comes from irregularities with sizes of the order of the Fresnel zone in the plane  $(x, y)$  perpendicular to the direction of propagation, which is much less than the outer scale. Thus the  $x, y$  dependence of the velocity can be neglected and restructuring of the scintillation pattern will be entirely due to the velocity variation along the propagation path. With this in mind the effective space-time spectrum of electron content fluctuations can be written as

$$S_{\Delta N_T}(\bar{\kappa}, \omega) = \phi_N(\bar{\kappa}) \int_0^L \delta(\omega + \bar{\kappa} \cdot \bar{v}(\xi)) d\xi / L \quad (10)$$

where the integral is taken along the propagation path of length  $L$  through the irregular layer and  $\bar{v}(\xi)$  is a function describing the velocity variation. Thus

the space-time spectrum is of the Shkarofsky's form with

$$\psi(\bar{\kappa}, \omega) = L \int_0^L \delta(\omega + \bar{\kappa} \cdot \bar{v}(\xi)) d\xi$$

A corresponding  $\psi(\bar{\kappa}, \tau)$  function is

$$\psi(\bar{\kappa}, \tau) = \frac{1}{L} \int_0^L e^{-i\tau \bar{\kappa} \cdot \bar{v}(\xi)} d\xi \quad (11)$$

In particular, if we assume that the velocity varies linearly along the propagation path, i.e.,  $\bar{v}(\xi) = \bar{v}_0 + \bar{v}_1 \xi/L$ , then

$$\psi(\bar{\kappa}, \tau) = \frac{1}{i\tau \bar{\kappa} \cdot \bar{v}_1} e^{-i\tau \bar{\kappa} \cdot \bar{v}_0} (1 - e^{-i\tau \bar{\kappa} \cdot \bar{v}_1}) \quad (12)$$

For  $|\tau \bar{\kappa} \cdot \bar{v}_1| \ll 1$ , (12) converges to the frozen field result (4).

These model spectra of nonfrozen irregularities will be applied in the following sections for the development of the correlation and dispersion analysis of spaced-receiver scintillation measurements.

### 3. MODELING AND CORRELATION ANALYSIS

To model temporal characteristics of scintillation we will adopt the phase screen theory, which has been shown to be satisfactory [Rino, 1979, 1982]. In our model, the screen is taken as located at  $z=0$ , in the middle of the irregularity slab. As the wave propagates to the ground, the phase mixing leads to the development of a complicated diffraction pattern whose statistics can be related to statistics of the phase on the screen, which in turn is related to the irregular structure of the ionosphere. For details of the theory the reader may consult a recent review by Yeh and Liu [1982]. For simplicity we assume that a plane wave of frequency  $f$  is incident normally onto the screen. The scintillation pattern is studied at a distance  $z$  below the screen. For a "shallow screen" such that the variance of the phase  $\phi_0^2 < 1$ , the space-time correlation function of the log amplitude  $\chi$  is given by

$$B_\chi(\bar{\rho}, \tau) = \iint_{-\infty}^{\infty} S_\phi(\bar{\kappa}_\perp, \tau) \sin^2(\kappa_\perp^2 z/2k) \cos(\bar{\kappa}_\perp \cdot \bar{\rho}) d^2 \kappa_\perp \quad (13)$$

where  $k=2\pi f/c$  is the wave number of the incident wave and  $S_\phi(\bar{\kappa}_\perp, \tau)$  is related to the two-dimensional spectral function of electron density fluctuations  $S_{\Delta N}(\bar{\kappa}_\perp, 0, \tau)$  by

$$S_\phi(\bar{\kappa}_\perp, \tau) = 2\pi L \lambda^2 r_e^2 S_{\Delta N}(\bar{\kappa}_\perp, 0, \tau) \quad (14)$$

In the above relation,  $L$  is the thickness of the irregularity layer,  $r_e$  is the classical electron radius ( $=2.818 \times 10^{-15}$  m) and  $\lambda=c/f$ .

Making use of the relations (2) and (5) the correlation function  $B_\chi(\bar{\rho}, \tau)$  can be put in the following form:

$$B_\chi(\bar{\rho}, \tau) = 2\pi L \lambda^2 r_e^2 \iint_{-\infty}^{\infty} \phi_{\Delta N}(\bar{\kappa}_\perp, 0) \sin^2(\kappa_\perp^2 z/2k) \cos[\bar{\kappa}_\perp \cdot (\bar{\rho} - \bar{v}_0 \tau)] e^{-\kappa_\perp^2 \Delta^2 / 2} d^2 \kappa_\perp \quad (15)$$

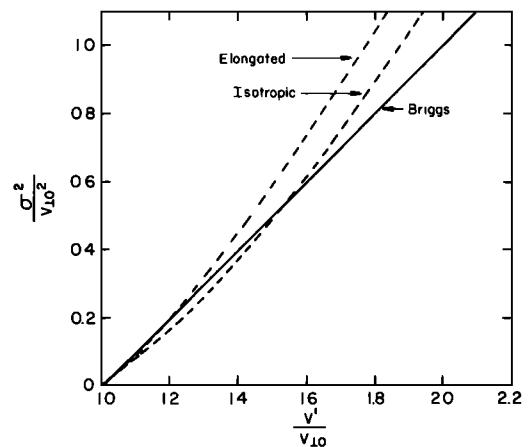


Fig. 1. Relationship between the apparent velocity  $v'$ , mean velocity  $v|_0$  and velocity variance  $\sigma$  for the model with elongated and isotropic irregularities and classical drift pattern analysis.

where  $\bar{v}_{\perp 0}$  represents the component of the mean velocity transverse to the direction of propagation.

We wish to relate the correlation function as given by equation (15) to the parameters measured with the spaced-receiver method. The most important parameter is the apparent velocity  $\bar{v}'$  defined as the ratio of the distance between the two receivers to the time lag  $\tau_m$  at which the cross-correlation is maximum. To find  $\tau_m$ , we compute first

$$\frac{\partial B_X}{\partial \tau} = 2\pi L\lambda^2 r_e^2 \int_{-\infty}^{\infty} \int_{-\infty}^{\infty} \phi_{\Delta N}(\bar{\kappa}_{\perp}, 0) \cdot \sin^2(\kappa_{\perp}^2 z/2k) \{(\bar{\kappa}_{\perp} \cdot \bar{v}_{\perp 0}) \cdot \sin[\bar{\kappa}_{\perp} \cdot (\bar{\rho} - \bar{v}_{\perp 0} \tau)] - \kappa_{\perp}^2 \Delta \frac{\partial \Delta}{\partial \tau} \cos[\bar{\kappa}_{\perp} \cdot (\bar{\rho} - \bar{v}_{\perp 0} \tau)]\} \cdot e^{-\kappa_{\perp}^2 \Delta^2/2} d^2 \kappa_{\perp} \quad (16)$$

For strictly frozen flow  $\Delta=0$ ,  $B_X(\bar{\rho}, \tau)$  reaches its maximum value at  $\tau_m$  such that  $\bar{\rho} = \bar{v}_{\perp 0} \tau_m$ . The apparent velocity is defined by  $\bar{v}' = \bar{v}_{\perp 0} / \cos \alpha = \bar{\rho} / \tau_m$ , where  $\alpha$  is the angle between  $\bar{\rho}$  and  $\bar{v}_{\perp 0}$ . If measurements at three nonlinear  $\perp_0$  receivers are available, then both  $\alpha$  and  $\bar{v}_{\perp 0}$  can be determined.

When  $\Delta$  is not constant and for a general propagation geometry, an analytical derivation of  $\tau_m$  and  $\bar{v}'$  is not possible. Numerical integration has to be used. However, approximate expressions can be obtained if  $\bar{\rho}$  is parallel to  $\bar{v}_{\perp 0}$ . If we write  $\tau_m = \bar{\rho} / \bar{v}_{\perp 0} + \delta\tau$ , where the additional time shift  $\delta\tau$  of the maximum caused by the nonfrozen property of the irregularities is assumed to be small, then it can be shown from (16) by a perturbation analysis that

$$\delta\tau \approx - \frac{2\Delta \frac{\partial \Delta}{\partial \tau}}{\bar{v}_{\perp 0}} \Big|_{\tau = \bar{\rho} / \bar{v}_{\perp 0}} \quad (17)$$

If the nonfrozen variation is caused by

the velocity fluctuations with standard deviation  $\sigma$ , the total time shift of the maximum,  $\tau_m$ , and the apparent velocity,  $\bar{v}'$ , are given respectively by

$$\tau_m = \frac{\bar{\rho}}{\bar{v}_{\perp 0}} \left(1 - 2 \frac{\sigma^2}{\bar{v}_{\perp 0}^2}\right) \quad (18)$$

$$\bar{v}' = \bar{v}_{\perp 0} \left(1 - 2 \frac{\sigma^2}{\bar{v}_{\perp 0}^2}\right)^{-1} \approx \bar{v}_{\perp 0} + 2 \frac{\sigma^2}{\bar{v}_{\perp 0}} \quad (19)$$

Expression (19) shows that the apparent velocity increases due to the velocity fluctuations. Compared with the formula derived by Briggs [1968a] which relates the apparent velocity to the mean drift velocity and characteristic random velocity  $v_c$

$$\bar{v}' = \bar{v}_{\perp 0} + \frac{v_c^2}{\bar{v}_{\perp 0}} \quad (20)$$

the meaning of  $v_c$  for the model is now straightforward:  $v_c^2$  is equal to a two-dimensional variance of the velocity fluctuations  $2\sigma^2$ . This result agrees with that obtained by Wright and Pitteway [1978] who simulated numerically the drift measurements. However, according to our discussion, it is valid only when the ratio  $\sigma^2 / \bar{v}_{\perp 0}^2$  is small. In general the relation between the apparent velocity and velocity fluctuation is more complicated.

Figure 1 shows the relation between  $\bar{v}' / \bar{v}_{\perp 0}$  and  $\sigma^2 / \bar{v}_{\perp 0}^2$  as derived from direct numerical computation of  $B_X(\bar{\rho}, \tau)$ . Two cases corresponding to isotropic and elongated irregularities are shown. The elongation is assumed to be perpendicular to the mean velocity and for this case  $\sigma^2$  is the one-dimensional velocity variance. Also shown is the relation (20) from Briggs' original derivation. In computing  $B_X(\bar{\rho}, \tau)$  it was assumed that the irregularity spectrum is of the power law type  $\kappa^{-p}$  with the outer scale much greater than the Fresnel zone size. It turns out that the curves shown in Figure 1 are almost independent of the spectral index  $p$ , the separation of the receivers  $d$ , the wave frequency and the distance  $z$ . This

figure shows that as ratio  $\sigma^2/v_{\perp 0}^2$  increases the characteristic random velocity  $v_c$  is no longer equal to the standard deviation of the velocity fluctuation.

Consider now the case when decay is caused by diffusion, so that  $\Delta = \sqrt{2D|\tau|}$ . function and the apparent velocity are given by

$$\tau_m = \frac{\rho}{v_{\perp 0}} - 2 \frac{D}{v_{\perp 0}^2} \quad (21)$$

$$v' = \frac{v_{\perp 0}}{1 - \frac{2D}{v_{\perp 0}^2}} \approx v_{\perp 0} \left(1 + \frac{2D}{v_{\perp 0}^2}\right)$$

Unlike for decay by velocity fluctuation, diffusion causes the apparent velocity to be dependent on the separation of the receivers. For large separation the effect of diffusion is small and the apparent velocity is close to the mean flow velocity.

Huba and Ossakow [1981] have shown that classical or anomalous diffusion for scintillation causing irregularities is very slow. It is easy to see, using numerical values given by Huba and Ossakow, for F region irregularities that for irregularities larger than 500 m the anomalous diffusion coefficient is smaller than 40 m<sup>2</sup>/s, which means that the additional time shift  $\delta\tau$  of the correlation function is less than 0.03 s for a typical value of mean velocity ( $\geq 50$  m/s). Therefore in most cases the effect of diffusion on the time lag for maximum correlation is negligibly small.

Velocity variations along the propagation path also cause the apparent velocity to deviate from the mean flow velocity. Numerical computation of  $B_{\chi}(\rho, \tau)$  for a linear velocity variation  $v(\xi) = v_0 + v_1 \xi/L$  shows that the following relation holds for the case of elongated irregularities with elongation in the direction perpendicular to the line joining the two antennas,

$$v' = \langle v_{\perp} \rangle + 0.0875 \frac{v_{\perp 1}^2}{\langle v_{\perp} \rangle} \quad (22)$$

where  $\langle v_{\perp} \rangle$  is the average transverse velocity equal to  $v_{\perp 0} + v_{\perp 1}/2$ .

In the correlation analysis, the so-called true velocity is obtained from the time shift  $\tau_c$  at which the autocorrelation and cross-correlation functions have the same value. Mathematically,  $\tau_c$  satisfies the relation

$$B_{\chi}(\bar{\rho}, \tau_c) = B_{\chi}(0, \tau_c) \quad (23)$$

From (15) one can easily see that  $\tau_c$  can be used to derive the mean flow velocity, as the relation

$$\bar{\rho} = 2v_{\perp 0} \tau_c \quad (24)$$

is valid independent of the form of the  $\Delta$  function. In the model with linear velocity variation along the propagation path  $v_{\perp 0}$  must be replaced by the average velocity  $v_{\perp 0} + v_{\perp 1}/2$  in (24).

We now turn our attention to the results of numerical computations. We concentrate mainly on the case when irregularities are infinitely elongated in the direction perpendicular to the line joining the two receivers. Such geometry is encountered at the equator, the case of interest here. Scintillation caused by isotropic irregularities will be also mentioned for comparison purposes.

For elongated irregularities, with a three-dimensional power law irregularity spectrum of the form  $\kappa^{-p}$  and a normal velocity distribution, (15) simplifies to

$$B_{\chi}(x, \tau) \sim \int_0^{\infty} \kappa_x^{-p+1} \sin^2 \left( \frac{\kappa_x^2 z}{2k} \right) \cos \left[ \kappa_x (x - v_{\perp 0} \tau) \right] e^{-\kappa_x^2 \tau^2 \sigma^2 / 2} d\kappa_x \quad (25)$$

where  $\sigma$  is the rms velocity. The above integral is defined for  $1 < p < 5$  and can be expressed in terms of the degenerate hypergeometric function  ${}_1F_1(a, b; x)$ :

$$B_{\chi}(x, \tau) \sim \Gamma\left(\frac{2-p}{2}\right) \left(\frac{z}{k}\right)^{\frac{p-2}{2}} \left\{ \eta^{\frac{p-2}{2}} e^{-\xi/\eta} \cdot {}_1F_1\left(\frac{p-1}{2}, \frac{1}{2}; \xi/\eta - \text{Re}[(\eta-1)] \frac{p-2}{2} e^{-\xi/(\eta-1)} \right) \right. \\ \left. {}_1F_1\left(\frac{p-1}{2}, \frac{1}{2}; \xi/(\eta-1)\right) \right\} \quad (26)$$

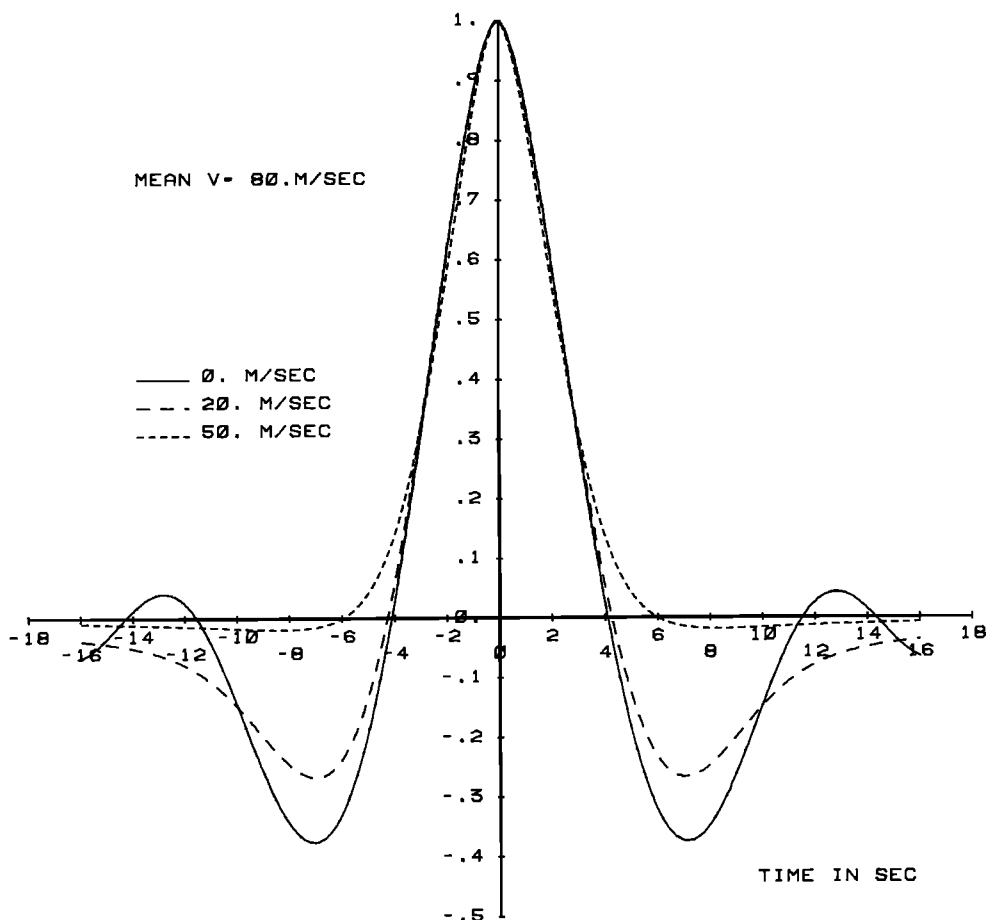


Fig. 2. Autocorrelation in the model with the normal velocity distribution, for three values of  $\sigma$ .

where  $\eta = \tau^2 \sigma^2 k / 2z$  and  $\xi = (x - v_{0x} \tau)^2 k / 4z$ .  
 At  $x=0, \tau=0$  the cross-correlation is given by

$$B_{\chi}(0,0) \sim \Gamma\left(\frac{2-p}{2}\right) \left(\frac{z}{k}\right)^{\frac{p-2}{2}} \cos\left[\frac{\pi(p-2)}{4}\right]$$

Thus for the normalized cross-correlation we have

$$R_{\chi}(x, \tau) = \left\{ \operatorname{Re}\left[ (\eta-i)^{\frac{p-2}{2}} e^{-\xi/(\eta-i)} \right] \right.$$

$$\left. {}_1F_1\left(\frac{p-1}{2}, \frac{1}{2}; \xi/(\eta-i)\right) \right\}$$

$$- \eta^{\frac{p-2}{2}} e^{-\xi/\eta} {}_1F_1\left(\frac{p-1}{2}, \frac{1}{2}; \xi/\eta\right) \left. \right\}$$

$$\div \cos\left[\frac{\pi(p-2)}{4}\right] \quad (27)$$

This expression has been used to calculate the cross-correlation for several values of the mean velocity  $v_{0x}$ , rms velocity  $\sigma$  and separation of the receivers  $x$ . In the computations,  $p=4.2$  and  $z=350$  km were assumed. Some examples are shown in Figures 2, 3 and 4. In Figure 2 the autocorrelation is depicted. One can see that fluctuating velocity mainly affects wings of the autocorrelation, destroying its oscillatory character related to the Fresnel oscillations. Figure 3 shows that velocity fluctuations have a more dramatic effect on the cross-correlation, not only reducing oscillations, but also introducing positive skewness which can be quite appreciable for large  $\sigma$ . In general, velocity fluctuations cause decorrelation of scintillation, i.e., a smaller peak value of the cross-correla-

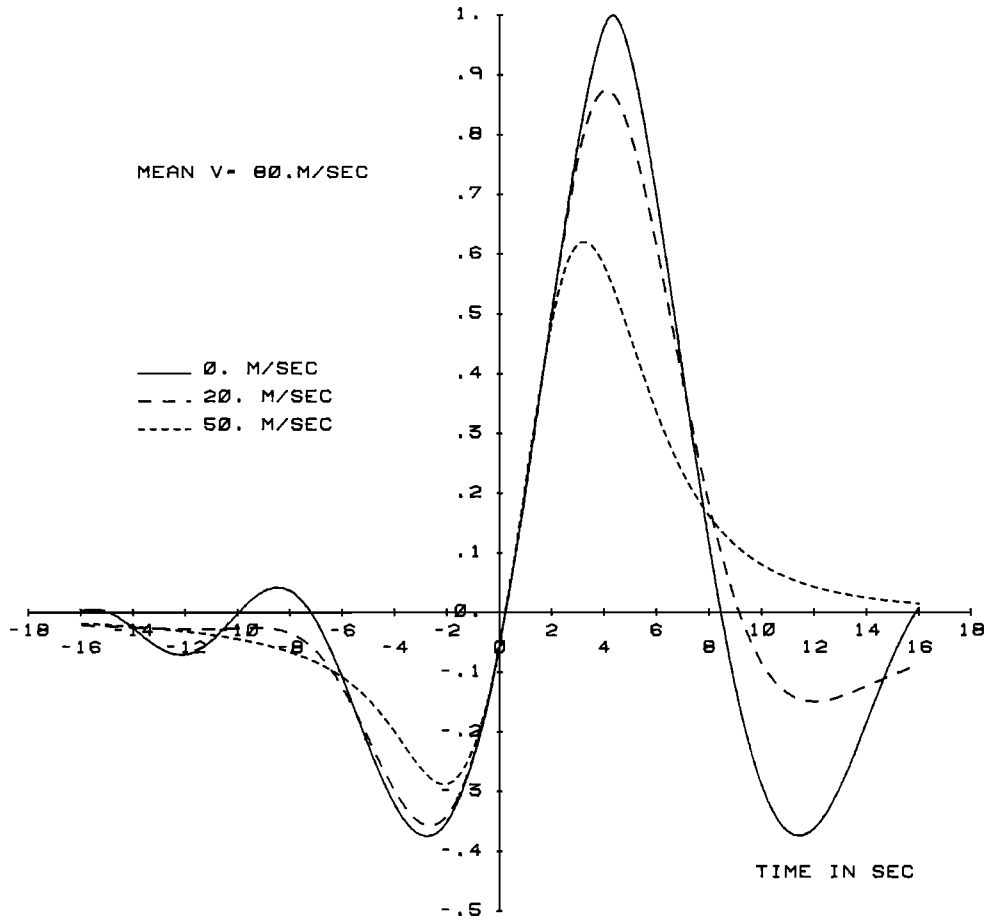


Fig. 3. Cross-correlation in the model with the normal velocity distribution, for three values of  $\sigma$ . Receiver separation is 366 m.

tion, and a shift of the peak toward a smaller time lag. This last effect is utilized in the correlation analysis to estimate  $\sigma$ . As Figure 1 shows, the correlation analysis underestimates velocity fluctuations if the ratio  $\sigma^2/v_{0x}^2$  is large. It is interesting to note that the slope of the cross-correlation at zero time lag is independent of  $\sigma$ .

Figure 4 shows how the cross-correlation changes with the separation of the receivers. The skewness increases, with increasing separation especially at large  $\tau - \tau_m$ , but it is always positive. At large separation, decorrelation is more pronounced.

For the case of linear velocity variation along the propagation path the normalized cross-correlation function can be expressed as

$$R_X(x, 0) = \int_0^L \{ \text{Re} [ (-i)^{\frac{p-2}{2}} e^{-i\xi} {}_1F_1 \left( \frac{p-1}{2}, \frac{1}{2}; i\xi \right) - \frac{\sqrt{\pi}}{\Gamma(\frac{p-1}{2})} \xi^{\frac{p-2}{2}} ] d\xi \} \quad (28)$$

where  $\xi = [x - v(\zeta)\tau]^2 k/4z$ .

Figures 5, 6, and 7 show results of calculations using (28) for  $v(\xi) = v_{0x} + v_{1x}\xi/L$ . It has been assumed that the scattering layer is 50 km thick. Changing the layer thickness and keeping  $v_{0x}$  and  $v_{1x}$  the same do not affect the results. Figures were constructed for the mean velocity equal to  $(v_{0x} + v_{1x})/2 = 80$  m/s. With the assumed layer thickness

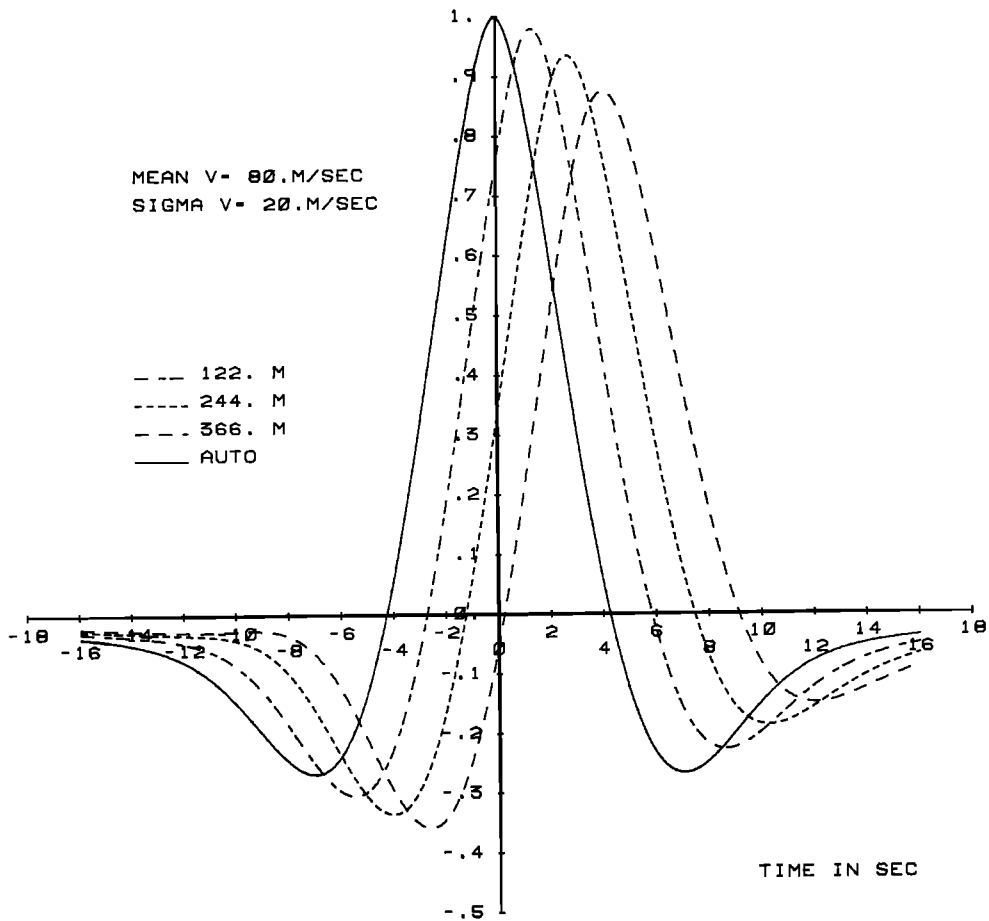


Fig. 4. Cross-correlation in the model with a normal velocity distribution, for different receiver separations.

the gradients 0.8, 1.4 and 2 m/s/km correspond to  $v_x = 60, 45, 30$  m/s and  $v_{1x} = 40, 70$  and  $100$  m/s, respectively. The corresponding rms velocities ( $=0.29v_{1x}$ ) are 11.5, 20.2 and 28.9 m/s.

Figures 5, 6 and 7 indicate that the velocity gradient along the propagation path has an effect on the cross-correlation similar to that of the velocity fluctuations. This conclusion is quite obvious, as in both models the correlation function is computed by averaging over the velocity. Therefore it is dependent on the moments of the velocity distribution rather than on its form. This means that it is not possible from a study of correlation function alone to distinguish between the effects caused by the velocity fluctuations and regular velocity variations along the propagation path.

#### 4. CROSS-SPECTRUM: DISPERSION ANALYSIS

The correlation analysis makes no provision for the possibility of a dispersive pattern motion when components of the pattern differing in scale sizes move with different velocities. In such cases a different type of analysis is required, in which a pattern is Fourier analyzed and a velocity of each Fourier component is calculated. An analysis of this type is called dispersion analysis. In practice, the phase of the cross-spectrum for a pair of records is computed as a function of the frequency  $f$ . It can be shown that this is equal to the phase difference between the Fourier components of the two records. If the Fourier component at frequency  $f$  is produced by the

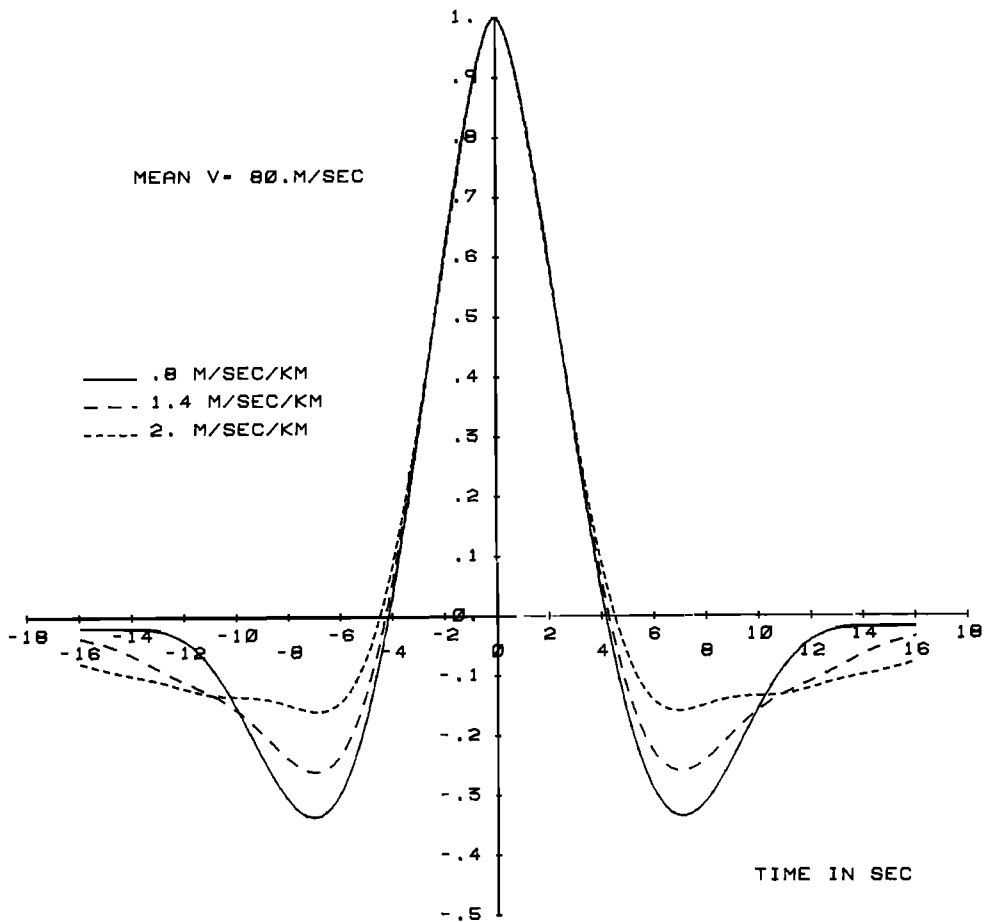


Fig. 5. Autocorrelation for three values of the velocity gradient along the propagation path. The gradient corresponds to a scattering layer 50 km thick.

passage of a sinusoidal wave over the receivers, the phase difference will be equal to  $2\pi f\rho/v_f$ , where  $\rho$  is the distance between the receivers and  $v_f$  is the phase velocity of the wave. Thus, from the measured phase of the cross-spectrum, the velocity of each wave can be found. As noted by Briggs [1968b] the assumption that a given frequency is produced by a single wave is very crucial. If several waves with the same wavelength but different directions of propagation are superimposed, the analysis will still give a certain velocity but it will not have the meaning of the phase velocity of a wave. A similar situation occurs when the waves move with a randomly fluctuating velocity.

Dispersion analysis has been used by

several authors [Briggs and Golley, 1968; Elkins and Papagiannis, 1970; Jones and Muade, 1972; Lotova and Chashey, 1977 a, b, 1978]. In most cases positive dispersion has been found, i.e., the velocity increases with frequency, eventually reaching certain asymptotic values at high frequencies. Briggs and Golley [1968] suggested that the positive dispersion might be caused by a regular velocity gradient along the propagation path. Elkins and Papagiannis [1970] have shown that dispersion of the direction of the velocity will lead to a dispersion of apparent velocity. Their explanation can account for both positive and negative dispersion. Lotova and Chashey [1977a, 1978] attempted to interpret dispersion in terms of the ran-

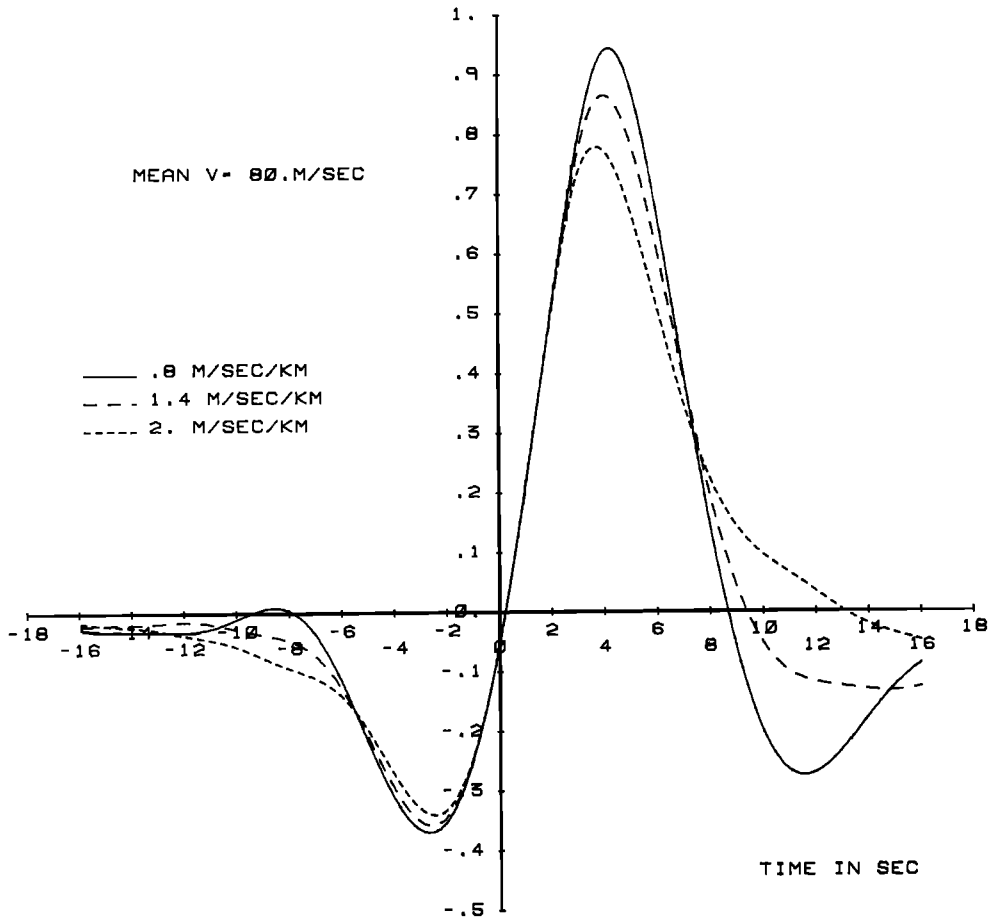


Fig. 6. Cross-correlation for three values of the velocity gradient along the propagation path. Receiver separation is 366 m.

domly fluctuating velocity of irregularities and eventually derived the parameters of the velocity distribution from measured  $v(f)$  curves.

To model the dispersion analysis of spaced-receiver measurements, the space-transformed with respect to time. For the decay mechanisms described by the function  $\psi(\bar{\kappa}, \tau)$  given in (5) the cross-spectrum  $P_\psi(\bar{\rho}, \omega)$  can be written as

$$P_\chi(\bar{\rho}, \omega) = 2\pi L \lambda^2 \tau e^2 \iint_{-\infty}^{\infty} \phi_{\Delta N}(\bar{\kappa}_\perp, 0) \cdot \sin^2(\kappa^2_\perp z/2k) \psi(\bar{\kappa}_\perp, \omega) e^{i\bar{\kappa}_\perp \cdot \bar{\rho}} d^2\kappa_\perp \quad (29)$$

where  $\psi(\bar{\kappa}_\perp, \omega)$  is the Fourier transform of  $\psi(\bar{\kappa}_\perp, \tau)$ .  
For a frozen flow with velocity  $\bar{v}_0$ ,

$$P_\chi(x, y, \omega) = 2\pi L \lambda^2 \tau e^2 \iint_{-\infty}^{\infty} \phi_{\Delta N}(\bar{\kappa}_\perp, 0) \cdot \sin^2(\kappa^2_\perp z/2k) \delta(\omega + \bar{\kappa}_\perp \cdot \bar{v}_0) \cdot e^{i\bar{\kappa}_\perp \cdot \bar{\rho}} d^2\kappa_\perp$$

$$= \frac{2\pi L \lambda^2 \tau e^2}{v_{0x}} \int_{-\infty}^{\infty} \phi_{\Delta N}(q_x, \kappa_y, 0) \cdot \sin^2(q^2 z/2k) e^{i(q_x + \kappa_y) y} d\kappa_y \quad (30)$$

where

$$q_x = \frac{\omega}{v_{0x}} + \kappa_y \frac{v_{0y}}{v_{0x}} \quad q^2 = q_x^2 + \kappa_y^2$$

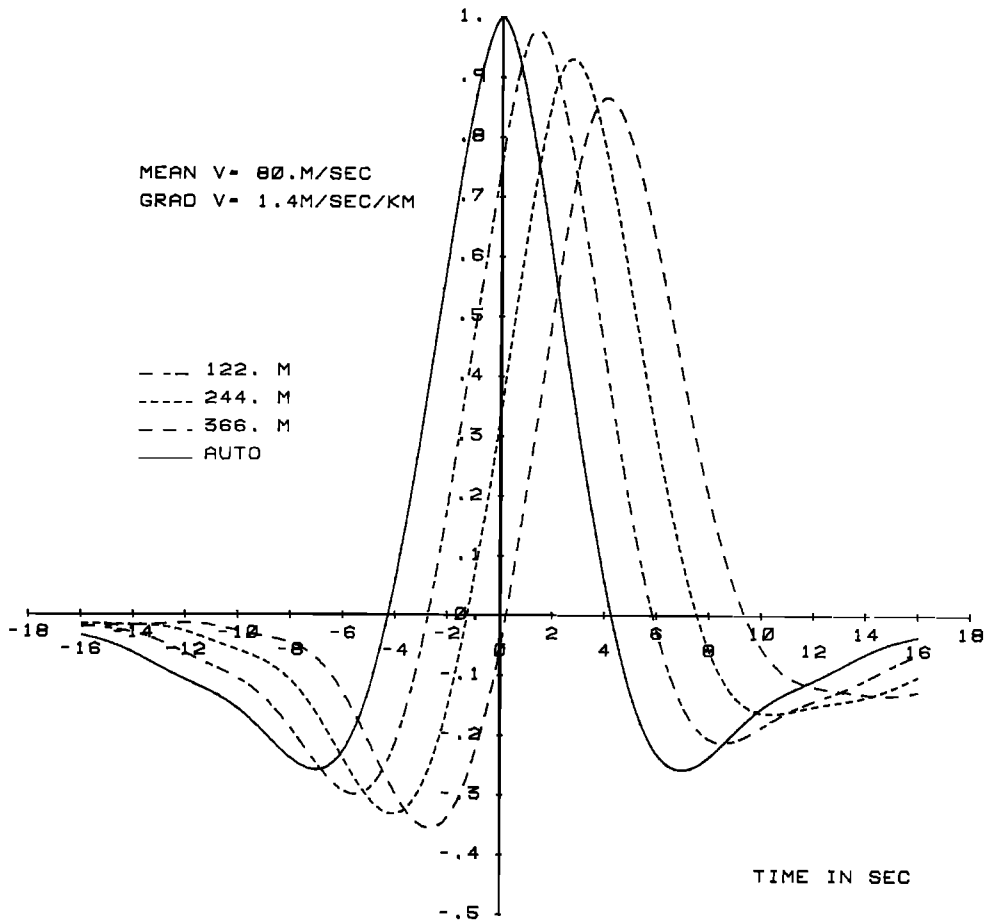


Fig. 7. Cross-correlation for a fixed velocity gradient along the propagation path and three different receiver separations.

Let us assume that the decay is due to the velocity fluctuations. Referring to (6) and the definition of characteristic function it can be found easily that

$$\psi(\bar{\kappa}_\perp, \omega) = \iint_{-\infty}^{\infty} \phi(\bar{v}) \delta(\omega + \bar{\kappa}_\perp \cdot \bar{v}_\perp) d^2v_\perp \quad (31)$$

with  $\phi(\bar{v})$  standing for the velocity probability distribution function. Substituting (31) into (29) and comparing with (30) we find that the cross-spectrum of scintillation in the situation of non-frozen flow due to the velocity fluctuations is equal to the cross-spectrum under the frozen flow assumption averaged over the velocity.

To simplify further discussion let us assume that the x axis is parallel to

the line joining two receivers and that the flow is one-dimensional, i.e.,  $\phi(\bar{v}) = \phi(v_x) \delta(v_y)$ . The cross-spectrum takes the form

$$P_\chi(x, \omega) = 2\pi L \lambda^2 r_e^2 \int_{-\infty}^{\infty} \phi(v_x) e^{iq_x x} \frac{dv_x}{v_x} \cdot \int_{-\infty}^{\infty} \phi_{\Delta N}(q_x, \kappa_y, 0) \sin^2(q^2 z / 2k) dk_y \quad (32)$$

where  $q_x = \omega/v_x$  and  $q^2 = q_x^2 + \kappa_y^2$ .

In the dispersion analysis the function of interest is the velocity  $v(\omega)$  defined as

$$v(\omega) = \frac{\omega x}{\alpha(\omega)} \quad (33)$$

where  $\alpha(\omega)$  is the phase of the cross-spec-

trum. It can be easily seen from (32) that for the  $\delta$  function type of the velocity distribution (frozen flow),  $\alpha(\omega) = \omega x / v_{0x}$ , and therefore  $v(\omega)$  is equal to the flow  $v_{0x}$ . The case of general distribution of  $v_x$  was discussed by Lotova and Chashey [1981].

Let us now discuss the situation when the velocity  $v_x$  varies along the propagation path. In this case,

$$P_{\chi}(x, \omega) = 2\pi\lambda\tau_e^2 \int_0^L \frac{e^{iq_x x}}{v_x(\xi)} d\xi \cdot \int_{-\infty}^{\infty} \phi \Delta N(q_x, \kappa_y, 0) \sin^2(q^2 z / 2k) d\kappa_y \quad (34)$$

where  $q_x = \omega / v_x(\xi)$  and  $q^2 = q_x^2 + \kappa_y^2$ .

Equations (32) and (34) will be used in the numerical computations of the cross-spectrum and the resulting phase function  $\alpha(\omega)$  can then be used for the dispersion analysis.

##### 5. COMPARISON OF THE MODEL WITH MEASUREMENTS

In this section we compare numerical modeling results described in the previous section with the spaced-receiver scintillation data taken at Ancon (11.71°S, 77.15°W) on March 29, 1977, using transmissions at 249 MHz from LES 9 satellite. Three receivers were aligned in the east-west direction. The receiver spacings were 122, 244 and 366 m, with the smallest spacing between the west (W) and middle (M) receivers. Because our model applies to weak scintillation, we have chosen the postmidnight segment of the data corresponding to the decaying stage of equatorial scintillation. The data were digitized with the sampling period 0.021 s and the segment analyzed was 2.5 min long. The scintillation index was  $S_4 = 0.5$ .

For each receiver the mean amplitude was subtracted and the difference normalized to the rms amplitude. Because the power spectrum of the original data shows effects of the satellite spin at frequencies higher than 5 Hz, the normalized amplitude was low-pass filtered

using a 6-pole Butterworth filter with the cutoff frequency 5 Hz. To eliminate the phase distortion introduced by the filter, the data were passed through the filter twice, in the direct and reversed order. To save computation time, the data were decimated by 4. The resulting records were used to compute three autocorrelation and three cross-correlation functions using the conventional method. Figure 8 shows the records as they appear after filtering. Figure 9 depicts the average autocorrelation and three cross-correlation functions.

The following procedures have been applied to derive the mean and apparent velocities. From the autocorrelation function and the three cross-correlation functions derived from the data, three crossover points where the autocorrelation function intersects the cross-correlation functions and three additional crossover points among the cross-correlation functions were found and the corresponding time lags were plotted as a function of distance  $\rho_1 + \rho_2$ , where  $\rho_1$  and  $\rho_2$  are the spacings of receivers (Figure 10). For the crossings between autocorrelation and cross-correlation,  $\rho_2 = 0$ . The straight line passing through the origin was least square fitted. The mean pattern drift velocity  $\langle v \rangle$  is obtained by taking the inverse of the slope of the line and similar procedure was used to estimate the apparent velocity  $v'$  using the plot of peak lag times versus receiver spacings. The inverse of the slope of the least square fitted straight line passing through the origin yields directly the apparent velocity. In the actual computations the time lags at the crossings were computed by fitting a second-degree polynomial to the segments of the correlation functions. This eliminates the error caused by the fact that the correlations are given at discrete time intervals.

With the mean and apparent velocities known, assuming either velocity fluctuation or velocity gradient, the rms velocity  $\sigma$  or  $v_1$  can be found from Figure 1 and (22), respectively. For the data segment under discussion,  $\langle v \rangle = 86$  m/s and  $v' = 91$  m/s; thus the rms velocity is 20 m/s or  $v_1 = 70$  m/s. Remembering

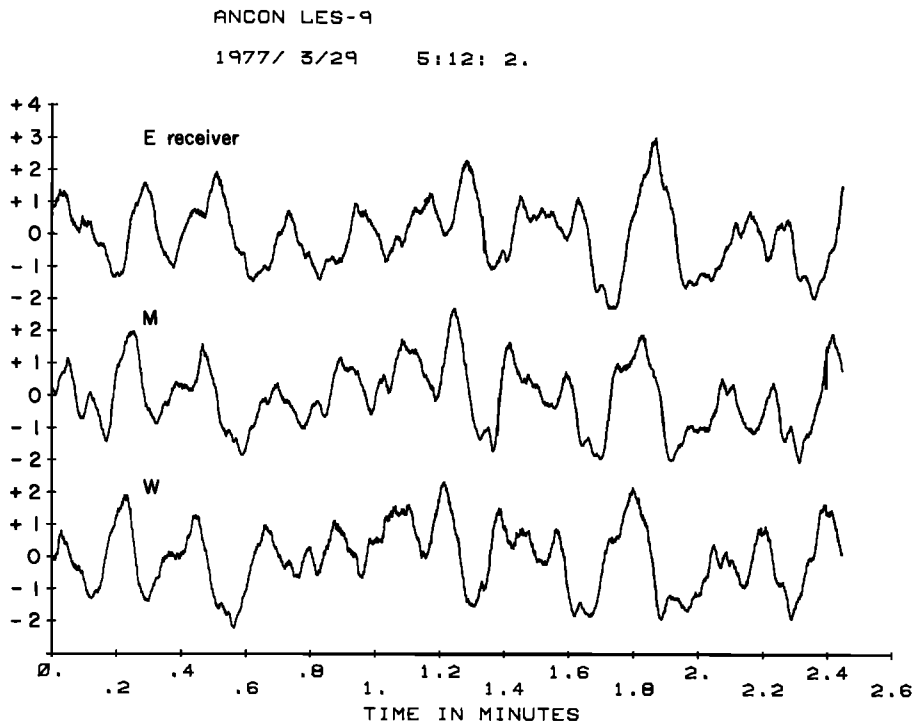


Fig. 8. Sample spaced-receiver amplitude records.

that  $\langle v \rangle = v_0 + v_1/2$  we obtain  $v_0 = 51$  m/s. The model assumes that the spectral index  $p$  and a distance  $z$  between the receiver and phase screen are known. The spectral index is estimated from the data in the usual way, using the log-log plot of the scintillation power spectrum. In Figure 11 the power spectra are depicted. In the frequency range from 0.2 to 1.2 Hz the average spectral index was found to be 4.2. Using these parameters, we can now compute the autocorrelation and cross-correlation functions for the three stations for the two models. A distance  $z=350$  km was chosen, as this gives the best agreement between the modeled and measured correlation functions. Figure 12 shows the measured and modeled autocorrelations and cross-correlations, for a receiver separation of 244 m. Only the model with the velocity gradient along the propagation path was shown for this comparison but the model with velocity fluctuations gives essentially the same picture. The velocity gradient corresponds to a scattering layer 50 km thick. From the figure, we see that the model

reproduces very well the main portion of the measured correlations. The peak cross-correlation predicted by the model is slightly higher than the measured value. This may be due to the fact that at  $S_4 \sim 0.5$  some decorrelation of scintillation, due to multiple scattering, is unable to reproduce the oscillations at large time lags. These oscillations indicate that the scintillation pattern is not exactly random, but some regular, large-scale periodic variations are present. Indeed, a closer inspection of the original and preprocessed amplitude records reveals the presence of periodicities with the period approximately 12-14 s. Discussion of this effect is beyond the scope of the present paper; we only mention that it might be caused by the wave diffraction on large-scale, regular electron density structures. The stochastic approach used to develop our model does not include effects caused by the regular structures.

The data segment was also spectrum analyzed. The three cross-correlations were Fourier transformed and the cross-

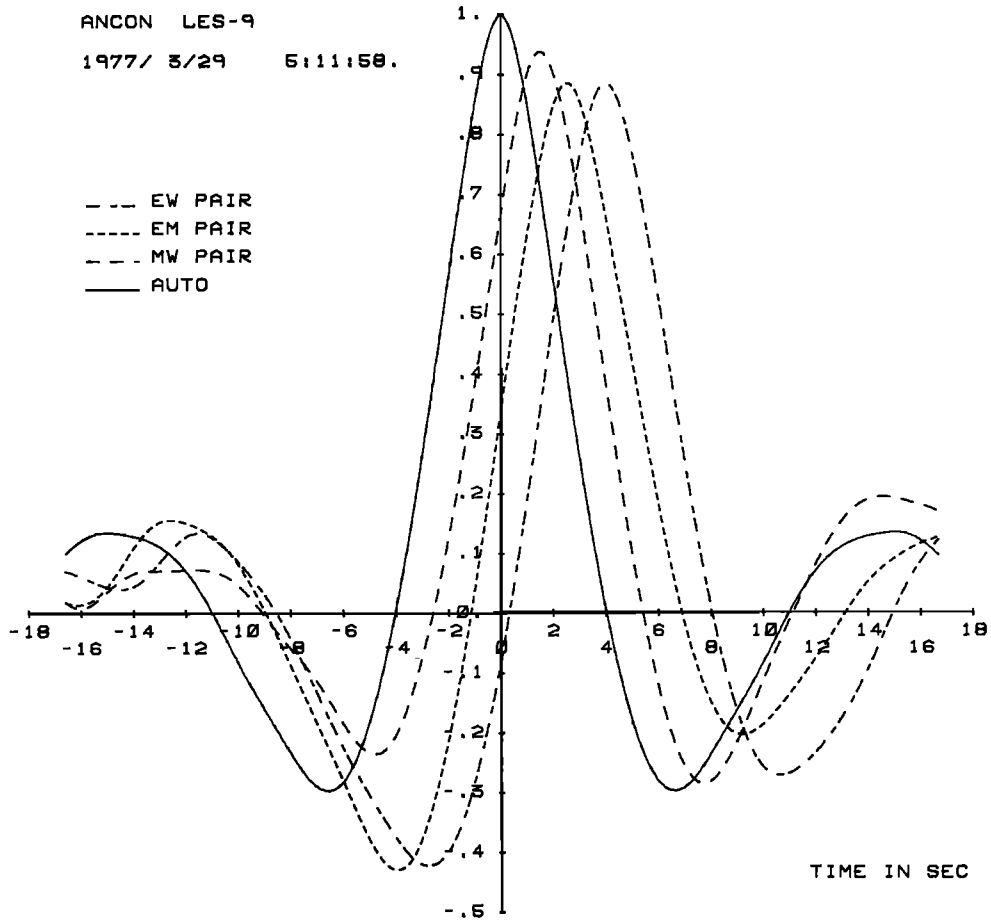


Fig. 9. Autocorrelation and cross-correlations computed for records shown in Figure 8.

phase  $\alpha(\omega)$  was determined as the arc tangent of the ratio of quadrature and in-phase components of the spectrum. The velocity dispersion function was obtained from (33). It must be noted that the variance of the phase increases if the coherency spectrum  $K^2$  [Jenkins and Watts, 1968] decreases:

$$\sigma_{\alpha}^2 \sim \frac{I}{2T} \left( \frac{1}{K^2} - 1 \right)$$

where  $I/T$  is the smoothing factor, controlled by the form of the window. The coherency spectrum is defined as

$$K^2(f) = \frac{|P_{12}(f)|^2}{P_1(f) \cdot P_2(f)}$$

$P_{12}$  is the cross-spectrum and  $P_1$  and  $P_2$  are the autospectra of scintillations recorded at each receiving point. In our calculations we used the Tukey window, the data segment is 1750 points long and number of lags 400, which gives  $I/T=0.17$ . Thus for  $K^2 < 0.5$  the rms phase is larger than 0.23. Therefore, only frequencies for which  $K^2 > 0.5$  were analyzed. This forced us to limit the analysis to frequencies less than 0.75 Hz.

The resulting velocity dispersion functions  $v(\omega)$  for each pair of receivers are shown in Figure 13. The general behavior of all three curves is similar, although the maximum at frequency 0.1-0.13, which approximately corresponds to the Fresnel frequency  $v_{0.1}/\sqrt{\lambda z}$ , is not so clearly visible for the pair of receivers with

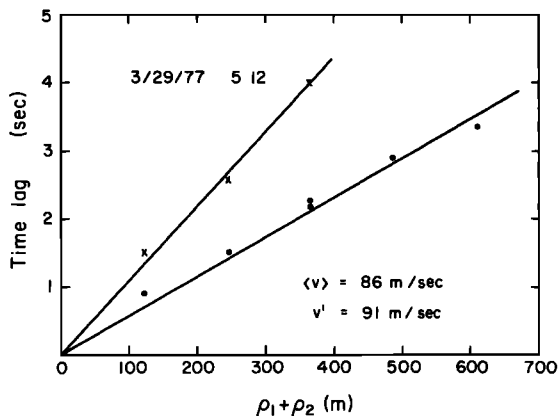


Fig. 10. Time lag of the peak cross-correlation and crossover time between auto-correlations and cross-correlations as a function of receiver separation.

the smallest spacing (MW pair). At high frequencies the curves tend to approach a constant value  $\sim 100$  m/s, eventually exhibiting some oscillations. Again, using the parameters obtained above, we computed the cross-spectra using (32) and (34). From these spectra,  $\alpha(\omega)$  and hence  $v(\omega)$  were obtained. The comparison between the model and measurements is shown in Figure 14 for the EM pair of receivers. The model with a constant velocity gradient was chosen for comparison, exactly the same as that used earlier for correlation modeling. We see that the main features, such as the maximum at the Fresnel frequency and the approximately constant  $v(\omega)$  at high frequencies [Lotova and Chashey, 1981], are reproduced by the model quite accurately.

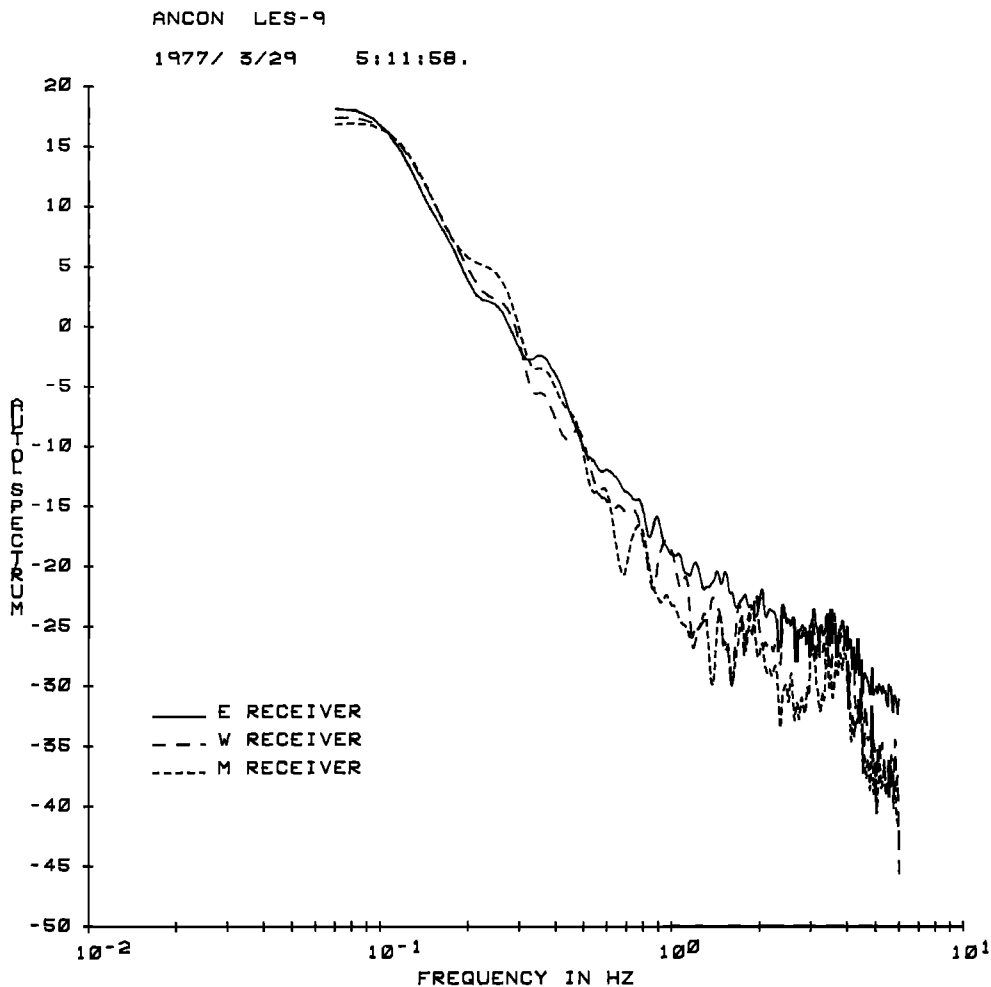


Fig. 11. Power spectra computed for the records shown in Figure 8.

ANCON LES-9

1977/ 3/29 5:11:58.

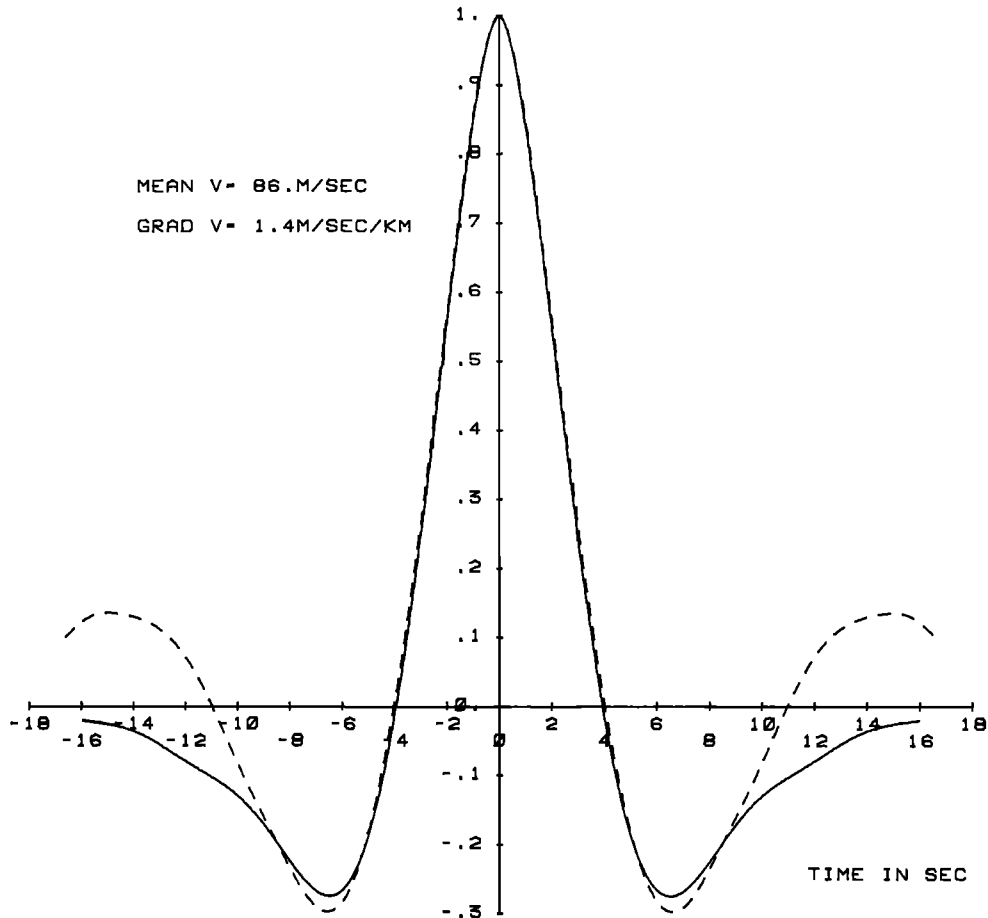


Fig. 12a. Comparison between the measured (dashed line) and modeled (solid line) autocorrelation for receivers separated by 244 m (ME pair).

## 6. CONCLUSIONS

We have shown that by applying scintillation theory together with appropriate irregularity models taking into account the processes responsible for the departure from the strictly frozen-in situation, one can effectively model the spaced-receiver scintillation experiments. First, correlation analysis of the scintillation is investigated. In the classical analysis of the drift patterns by the full correlation method as discussed by

Briggs et al. [1963], no assumptions were made about the physical mechanisms under which the drift patterns are formed. The only assumption is a mathematical one concerning the dependence of the correlation function on the spatial coordinates and the time, namely, that the correlation functions  $B_{\chi}(\rho, \tau) = \text{const}$  form concentric ellipsoids.<sup>χ</sup> In our model, the correlation functions are actually computed from scintillation theory, relating them to physical parameters such as the rms velocity  $\sigma$  and the velocity gradient  $\nabla v$ . The rela-

ANCON LES-9

1977/ 3/29 5:11:58.

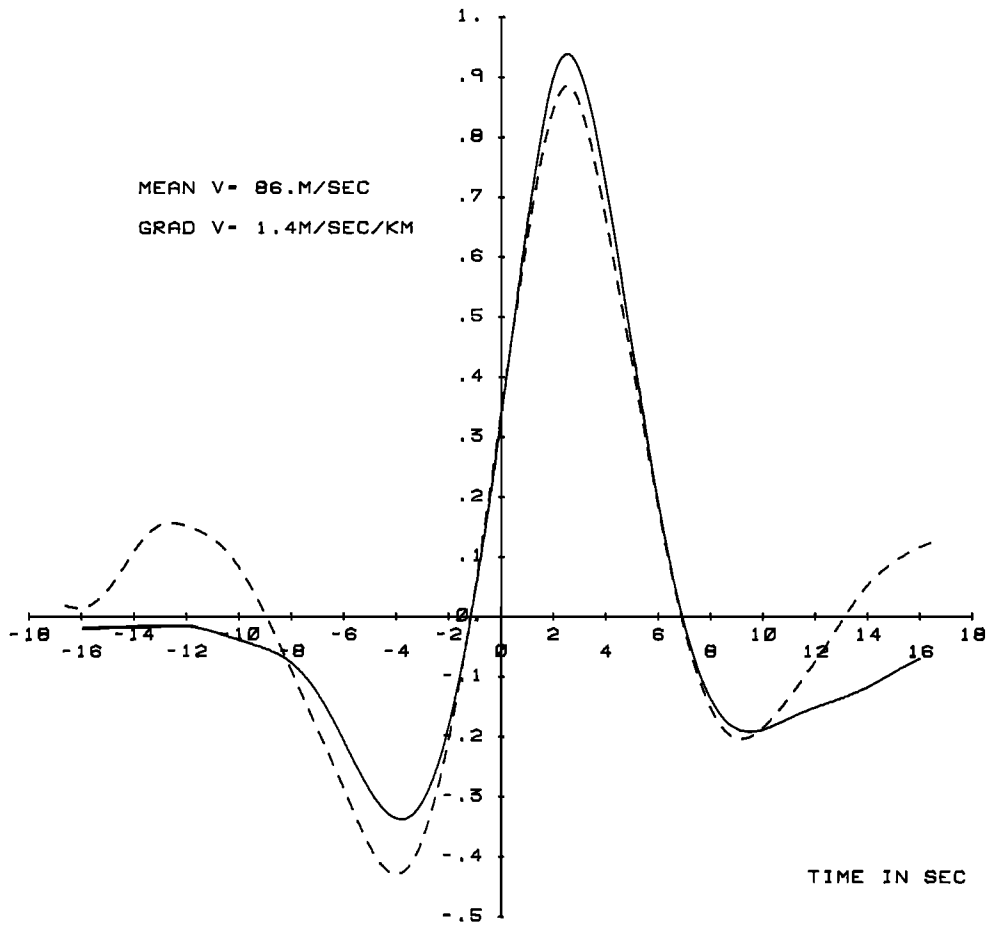


Fig. 12b. Same as Figure 12a except for cross-correlation.

ANCON LES-9  
1977/ 3/29 5:11:58.

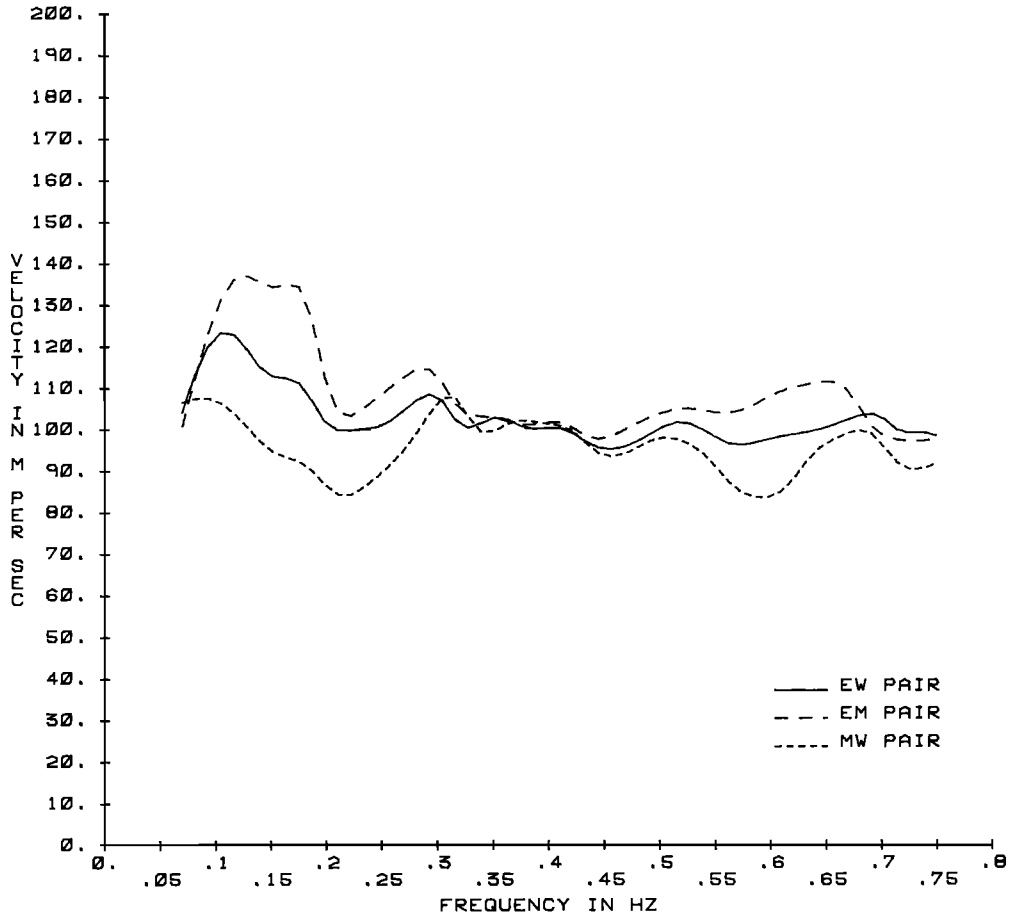


Fig. 13. Velocity dispersion function computed for sample records shown in Figure 8.

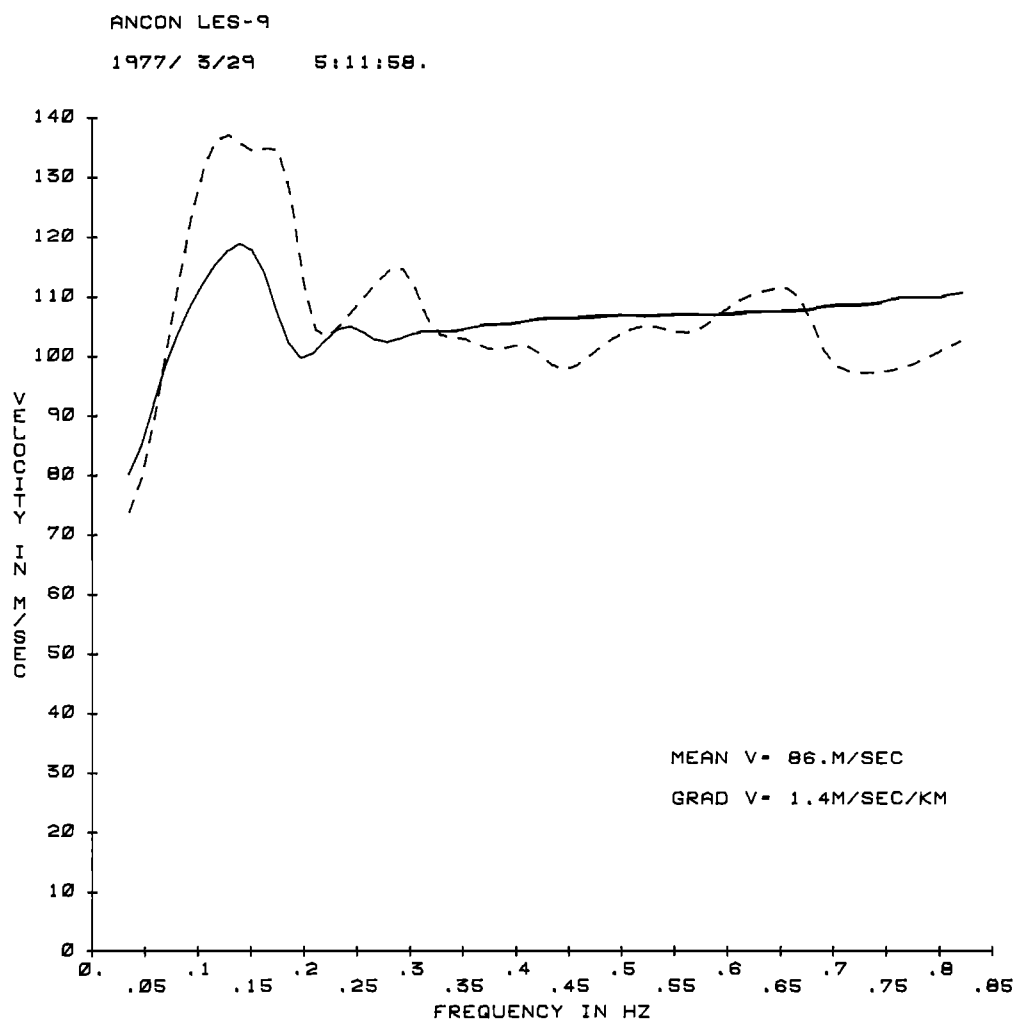


Fig. 14. Comparison between the measured (dashed line) and modeled (solid line) velocity dispersion function for receivers separated by 244 m.

relationship between  $\sigma$  (or  $\nabla v$ ) and the characteristic velocity  $v_0$  in the classical analysis is derived in this study. It is shown that from correlation analysis alone, it is not possible to distinguish between effects arising from random velocity fluctuation, and from variation of drift velocity along the propagation path. we also modeled the dispersion analysis using the cross-spectrum of the spaced signals. The dispersion analysis may be useful if the motion of the irregularities is truly dispersive, i.e., irregularities of different sizes move at different velocities.

Applying the modeling results to a set

of observational data, we have demonstrated that self-consistent models with either velocity fluctuations or velocity gradient can be constructed that yield excellent agreements between computed results and those from the observational data. Thus the modeling technique seems to have the potential to yield important information about the velocity fields in the ionosphere using spaced-station scintillation data.

The derivation in this paper is based on weak scintillation theory. For situations of strong scattering, the derivation has to be modified. The procedure will still be the same but the computations will be-

come more involved. It is expected, however, that some of the main features of our results may still be valid.

**Acknowledgments.** We thank H. E. Whitney of AFGL and Santimay Basu of Emmanuel College for providing us with the Ancon data. The computer programs used to decode, calibrate and preprocess the data were developed by J. Austen and S. Franke. The work was supported in part by a grant ATM 82-08931 from the Atmospheric Research Section, National Science Foundation.

#### REFERENCES

- Briggs, B. H., On the analysis of moving pattern in geophysics, I, Correlation analysis, J. Atmos. Terr. Phys., 30, 1777-1788, 1968a.
- Briggs, B. H., On the analysis of moving pattern in geophysics, II, Dispersion analysis, J. Atmos. Terr. Phys., 30, 1789-1794, 1968b.
- Briggs, B. H., Ionospheric drifts, J. Atmos. Terr. Phys., 39, 1023-1034, 1977.
- Briggs, B. H., and M. G. Golley, A test for dispersion in F-region drifts observed by the radio star scintillation method, J. Atmos. Terr. Phys., 30, 963-973, 1968.
- Briggs, B. H., G. J. Phillips, and D. H. Shinn, The analysis of observations on spaced receivers of the fading radio signals, Proc. Phys. Soc. London, 63, 106-121, 1950.
- Chashey, I. V., and V. I. Shishov, Nature of small-scale solar wind inhomogeneities, Geomagn. Aeron., Engl. Transl., 17, 1-4, 1977.
- Ekers, R. D., and L. T. Little, The motion of the solar wind close to the sun, Astron. Astrophys., 10, 310-316, 1971.
- Elkins, T. J., and M. D. Papagiannis, Dispersive motions of ionospheric irregularities, J. Atmos. Terr. Phys., 32, 383-395, 1970.
- Fedor, L. S., A statistical approach to the determination of three-dimensional ionospheric drifts, J. Geophys. Res., 72, 5401-5415, 1967.
- Huba, J. D., and S. L. Ossakow, Diffusion of small-scale density irregularities during equatorial spread-F, J. Geophys. Res., 86, 9107-9114, 1981.
- Jankins, G. M., and D. G. Watts, Spectral analysis and its applications, Holden-Day, San Francisco, Calif., 1968.
- Jones, D., and A. D. Maude, Dispersive motions in the ionosphere, J. Atmos. Terr. Phys., 34, 1241-1259, 1972.
- Kent, G. S., and R. W. H. Wright, Movements of ionospheric irregularities and atmospheric winds, J. Atmos. Terr. Phys., 30, 657-691, 1968.
- Little, L. T., and R. D. Ekers, A method for analyzing drifting random pattern in astronomy and geophysics, Astron. Astrophys., 10, 306-309, 1971.
- Lotova, N. A., and I. V. Chashey, Fine structure of solar-wind velocity distribution, Geomagn. Aeron., Engl. Transl., 13, 846-852, 1973.
- Lotova, N. A., and I. V. Chashey, Dynamics of the interplanetary plasma according to the data on temporal scintillation spectra, Geomagn. Aeron., Engl. Transl., 16, 137-140, 1976.
- Lotova, N. A., and I. V. Chashey, Dispersion analysis of the solar wind velocity, Izv. Vyssh. Uchebn. Zaved. Radiofiz., 20, 329-336, 1977a.
- Lotova, N. A., and I. V. Chashey, Nature of the temporal restructuring of the interplanetary scintillation pattern, Geomagn. Aeron., Engl. Transl., 17, 127-130, 1977b.
- Lotova, N. A., and I. V. Chashey, Velocity medium, according to scintillation observations, Geomagn. Aeron., Engl. Transl., 18, 553-557, 1978.
- Lotova, N. A., and I. V. Chashey, Velocity distribution in the scintillation pattern and the jet structure of the solar wind, Geomagn. Aeron., Engl. Transl., 21, 320-323, 1981.
- Rino, C. L., A power law phase screen model for ionospheric scintillation, 1, Weak scatter, Radio Sci., 14, 1135-1145, 1979.
- Rino, C. L., On the application of phase screen models to the interpretation of ionospheric scintillation data, Radio Sci., 17, 855-867, 1982.
- Rino, C. L., and R. C. Livingston, On the analysis and interpretation of spaced-receiver measurements of transionospheric radio waves, Radio Sci., 17, 845-854, 1982.

- Shkarofsky, I. P., Turbulence functions useful for probes (space-time correlation) and for scattering (wave-number-frequency spectrum) analysis, Can. J. Phys., 46, 2683-2702, 1968.
- Tatarski, V. I., The effects of the turbulent atmosphere on wave propagation, U.S. Dep. of Commerce, Nat. Tech. Inf. Serv., Springfield, Va., 1971.
- Wright, J. W., M. L. V. Pitteway, Computer simulation of ionospheric radio drift measurements, and their analysis by correlation methods, Radio Sci., 13, 189-210, 1978.
- Yeh, K. C., and C. H. Liu, Radio wave scintillation in the ionosphere, Proc. IEEE, 70, 324-360, 1982.
- 
- C. H. Liu and K. C. Yeh, Department of Electrical Engineering, University of Illinois at Urbana-Champaign, Urbana, IL 61801.
- A. W. Wernik, Space Research Center, Polish Academy of Sciences, Warsaw, Poland.